Kinetics of Individual Block Copolymer Island Formation and Disappearance near an Absorbing Boundary

Jakob Heier, Edward J. Kramer,* Jan Groenewold, and Glenn H. Fredrickson

Departments of Materials and Chemical Engineering, University of California, Santa Barbara, California 93106

Received September 28, 1999; Revised Manuscript Received April 14, 2000

ABSTRACT: We investigate the formation and coalescence of surface relief structures in symmetric diblock copolymers films of poly(styrene-*b*-2-vinylpyridine) (PS−PVP) on chemically patterned surfaces. The substrates have patterns of self-assembled monolayers (SAMs) produced by microcontact printing HO-terminated (HO−) SAM stripes alternating with H_3C-terminated (H_3C−) SAM stripes. The PS−PVP lamellae over the H_3C−SAM have a defect-rich morphology compared to the film above the HO−SAM. These film sections above the H_3C−SAM attract excess PS−PVP that would normally form islands on a uniform substrate. In the early stages of annealing waves of thickness develop from the H_3C/HO−SAM boundary and propagate into the film over the HO−SAM. For a 3 μm wide HO−SAM stripe a single line of excess copolymer breaks up into a single line of islands with a well-defined spacing along the grating. At long times these islands dissolve by transport of copolymer to the H_3C−SAM stripe. The well-defined 2D geometry allows us to analyze the transport leading to this dissolution quantitatively. The rate-controlling process during the island dissolution is two-dimensional pressure relaxation.

Introduction

The potential use of block copolymers as thin-film adhesives, surface-modifying agents in polymer blends, and interfacial agents in high-impact plastics has drawn an increasing interest in their surface and interface properties. In general, the interplay between connectivity and phase separation leads to a variety of bulk morphologies.[1] In the case of symmetric diblock copolymers, lamellar microdomains of period L_0 are formed. Interfaces can align the lamellae parallel to the substrate. In thin films under the influence of two interfaces only certain initial film thicknesses result in a flat film upon annealing. When both surfaces attract the same block, this thickness is $H = nL_0$. When the two boundary surfaces attract different blocks, flat films are found for $H = (n + {}^1/_2)L_0$. Deviations from these quantized values will lead to surface relief structures that appear on top of the flat films.[2−5] The most studied situation is a surface populated by an ensemble of islands or holes ("domains") as found after the initial stage of island/hole nucleation. Nucleation sites are statistically distributed over the sample surface. Typically, the average size of the domains increases through growth, coalescence, and dissolution of individual domains. The driving force for the coarsening is the domain edge line tension, leading to a decrease of the total length of the domain edges. The characteristic dimensions of the relief structures versus annealing time follow a power law ($R \propto t^{\alpha}$), but it has been extremely difficult to match theoretical predictions with the experimental observations.[6] Most theoretical models do not take the molecular structure of the diblock copolymers into account. Thus, a unique growth exponent of $\alpha = {}^1/_3$ (Lifschitz−Slyozov coarsening)[7] is predicted, while the values reported in most of the experiments lie far below this. A first molecular description for an ideal thin diblock copolymer film stresses that the following three mechanisms are competing in the evolution of the relief structures,[8] all leading to different exponents: (A) diffusional motion of the domains as a whole; (B) tunnel penetration of individual block copolymers into neighboring layers; (C) collective relaxation of the block copolymer due to viscous flows inside coherent layers. In Nyrkova and Semenov's picture[8] processes B and C are connected: Relaxation of an island can occur by first tunneling of copolymer molecules into the underlying layer followed by two-dimensional pressure relaxation inside this layer. Different domain edge structures, e.g., defect structures as proposed by Carvalho and Thomas,[9] may allow polymer to flow into the underlayer, making tunneling unnecessary.

Grim et al.[10] extended this description to the case of films containing defects, showing how the presence of defects can significantly lower the critical exponents. It is the poor knowledge of the distribution of defects and the variety of processes and mechanisms possible which frustrates the predictive understanding of the factors that determine the morphology evolution. For a further understanding it is necessary to create model shapes in which theory and experiment can be compared. In our approach we develop islands next to an excess copolymer-absorbing boundary. This situation can be realized experimentally by annealing the copolymer film on chemically structured substrates, to be more precise: alternating stripes of HO-terminated self-assembled monolayers (HO−SAMs) and H_3C-terminated monolayers (H_3C−SAMs). These films show a unique feature when studied as a function of film thickness:[11] additional block copolymer layers are preferentially formed on top of the H_3C−SAM. Note that this phenomenon is quite different from that where the block copolymer periodicity is matched by a chemical pattern[12] and from cases where SAM patterns have been used to direct the phase separation of polymer blends in solution[13] or in the melt.[14] We explain this phenomenon through the different morphologies of the block copolymer films forming on different substrates: On the HO−SAM, the lamellae are perfectly oriented parallel

* To whom correspondence should be addressed.

10.1021/ma991649v CCC: $19.00
Published on Web 07/12/2000

to the substrate with the PVP wetting the substrate and PS wetting the vacuum interface. In contrast, the alignment kinetics on the H_3C-SAM is dramatically slowed as a consequence of the compensating attractions of the PS to the H_3C-SAM and the PVP to the underlying gold layer where there are defects in the monolayer. For long annealing times, the layer shows regions where lamellae are aligned parallel as well as those where the orientation is perpendicular to the substrate. Accumulation of excess material is more favorable on unaligned lamellae or defect-rich structures compared to a complete and defect-free lamellar film. Excess domains can lower their edge free energy on a defect-rich surface. Islands initially formed on the HO-terminated substrate in this way uniquely decay and are absorbed by the film on the H_3C-terminated thiol in a late coalescence stage. The substrate patterning also reveals interesting details on the very early stages of domain formation. The surface roughening now has directionality and waves of thickness develop from the H_3C/HO−SAM stripe boundary into the HO−SAM. In a first part we describe the sample preparation and characterization. We then discuss the formation and dissolution of individual islands in more detail, and we present a model describing islands next to an absorbing stripe boundary.

Experimental Section

The system under investigation is a poly(styrene-*b*-2-vinylpyridine) (PS−PVP) diblock copolymer with equal indices of polymerization of the blocks ($N_{PS} \cong 960$ and $N_{PVP} \cong 960$), which forms lamellar microdomains. The polymers were synthesized via anionic polymerization.[15] From the height of islands and holes in thin films as well as from cross-sectional transmission electron microscopy (TEM) in bulk samples, we determined the equilibrium lamellar thickness to be $L_0 = 69$ nm. Patterned self-assembled monolayers (SAMs) were formed by microcontact printing[16] of functionalized alkanethiols on a gold-coated silicon wafer. Lines of H_3C-terminated thiols were transferred onto the Au surface by use of a microfabricated elastomer stamp. Subsequently, the substrate was immersed into a solution of HO-terminated thiol, allowing the monolayer to form in the empty spaces between the lines of the H_3C-terminated SAM. Films of PS−PVP 120 nm ($1.7L_0$) thick were spun cast onto the patterned substrates from toluene solution. The films were annealed in a high-vacuum ($\sim 7 \times 10^{-5}$ Pa) furnace at 176 °C for various times. The topography was imaged with scanning force microscopy (SFM) with a Nanoscope III from Digital Instruments in contact mode. We performed all of our measurements with a Si_3N_4 cantilever tip with a force constant of 0.06 N m^{-1}. Island areas were measured using the "Bearing" tool of the Nanoscope III software analysis program. The block morphology of the film can be made visible with transmission electron microscopy (TEM). To improve contrast, the PVP was stained by exposure to iodine vapor for 4−6 h.

Results

After spin-casting the surfaces of the sample are flat (rms roughness 2 nm). On a homogeneous substrate the surface shows increasing roughening upon annealing until domains L_0 in height are formed. By introducing a chemical substrate pattern, we exploit the tendency for the system to decompose into a film with two coexisting thicknesses to create a well-defined island pattern. The H_3C/HO−SAM boundary plays a major role in the pattern formation process. Excess copolymer does not form an isotropic pattern of islands and holes as on a homogeneous substrate. In this case it is energetically favorable to accumulate additional copolymer chains on top of the H_3C-SAM as the film on top of the H_3C-SAM has a defect-rich lamellar structure. General results for the kinetics of coarsening of block copolymer islands on thin block copolymer films have been published by Grim et al.[10]

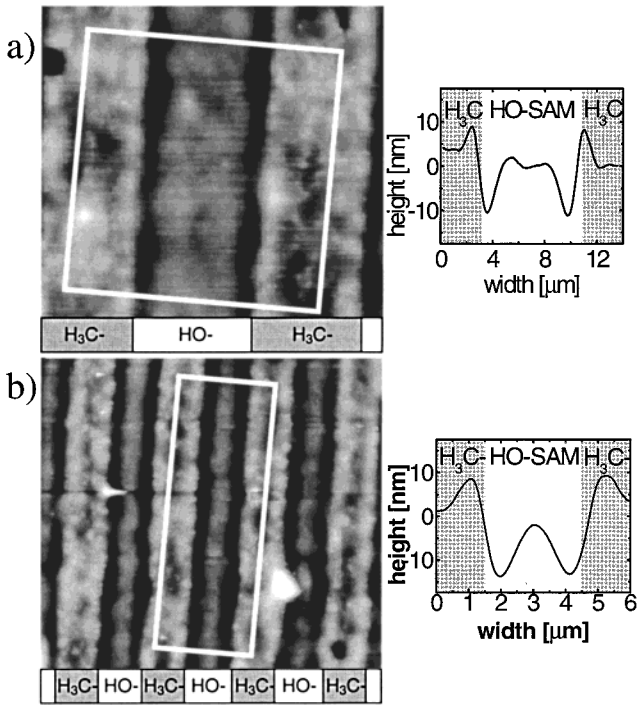

Figure 1. Surface topography of a $1.7L_0$ thick PS−PVP film annealed at 176 °C for 20 min on gratings consisting of HO−SAM stripes alternating with H_3C-SAM stripes. In (a) we show a grating with an HO−SAM stripe width of 7 μm, and in (b) we show a grating of an HO−SAM stripe width of 3 μm. The base side of the SFM images is 20 μm. On the right side of the SFM images we plot averaged cross sections perpendicular to the grating over an area indicated by the white squares.

Already for the shortest annealing times some copolymer is transferred across the H_3C/HO SAM boundary from the film above the HO−SAM to the film above the H_3C-SAM. After 10 min of annealing we find a ridge of excess polymer on the H_3C-SAM side of the boundary and a trench on the HO−SAM side of the boundary. As shown in Figure 1, excess copolymer stripes of different width are left on top of HO−SAM stripes of different width. If we choose a special width of the HO−SAM stripe, the excess material ridge in the middle of the HO−SAM stripe breaks up into a single line of "island" droplets upon further annealing. This scenario is realized for a HO−SAM stripe width of 3 μm. We show the time evolution of this island structure in Figure 2.

For much smaller HO−SAM stripe widths no isolated islands form on top of the HO−SAM. All the excess copolymer is transported to the H_3C-SAM. Gratings of much larger HO−SAM stripe width show more or less isotropic domain growth on top of the HO−SAM stripe. We reported in earlier experiments[17] that islands are preferentially located at certain repeat distances from the wall (1.5, 3.5, and 5.5 μm).

We now undertake a more detailed description of the process leading to the island formation (Figure 2). The excess copolymer ridge in the middle of the HO−SAM stripe (Figure 2a) has not yet reached a height L_0, the height of an equilibrium large lamellar island. Upon

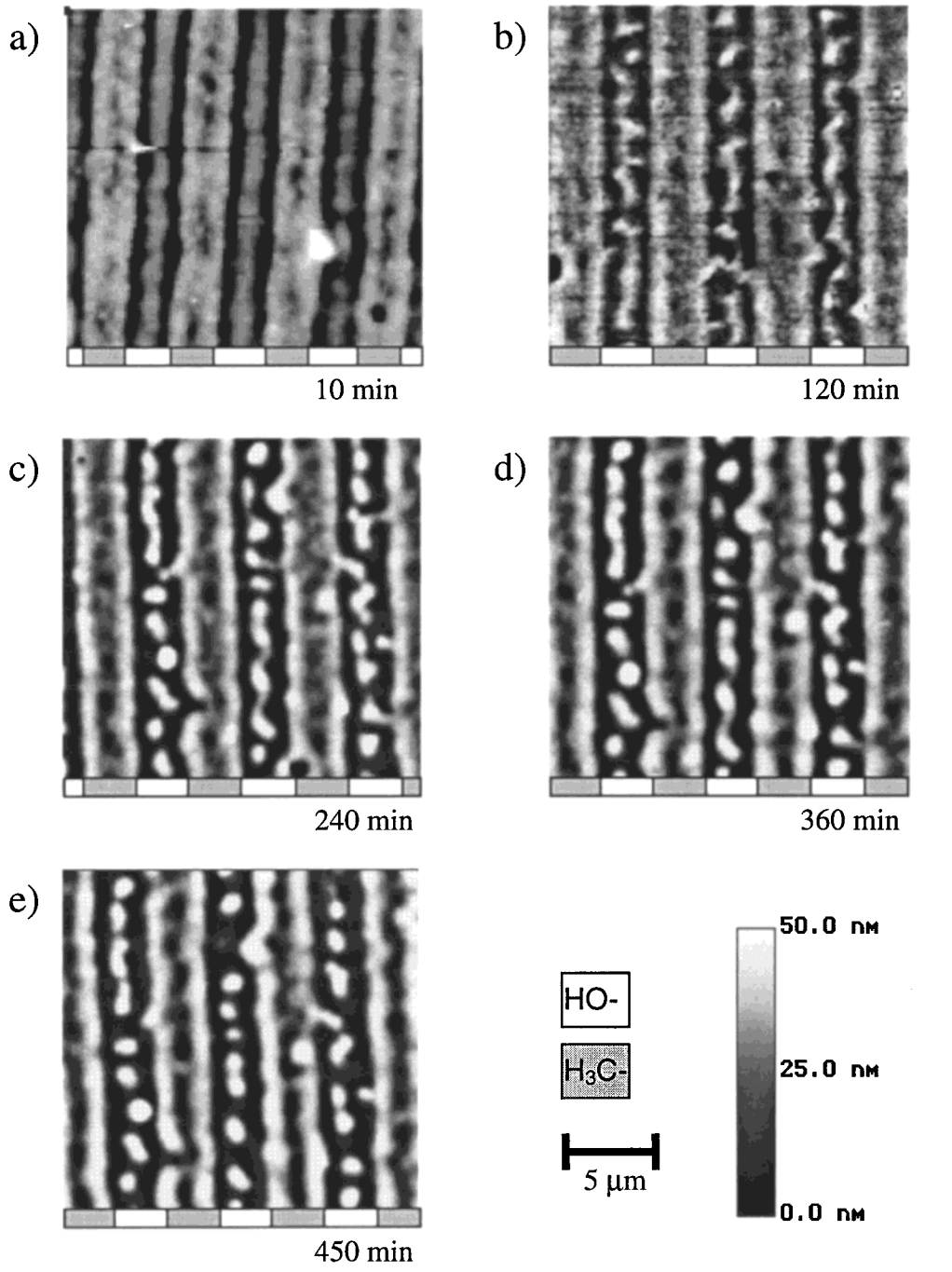

Figure 2. SFM images of a thin film of PS−PVP on a grating with about 6 μm periodicity (~3 μm HO−SAM stripe width) annealed for different times at 176 °C. Images b−e are from the same region of the same film while (a) was from a different film with a grating of similar but slightly different periodicity.

annealing the height of the midstripe ridge increases, and we observe a thinning of the ridge accompanied by in-plane modulations (Figure 2b). In the next stage (Figure 2c−e) we also observe height modulations within this ridge that lead eventually to a breakup of the ridge into individual islands. Remarkably, these islands are arranged along the grating with a certain spacing. There is a distinct peak at wavevector $k_x = 2.8$ μm^{-1} in the one-dimensional Fourier transform of the SFM image of the HO−SAM stripe in a direction along the grating as seen in Figure 3. This regular spacing of the islands suggests that the breakup of the ridge results from an instability similar to the well-known Rayleigh instability.[18] Lord Rayleigh showed that for a cylinder of an inviscid liquid perturbations with a greater wavelength than a certain threshold value will continue to increase in magnitude until the cylinder breaks up into a line of droplets with the spacing of this wavelength. We expect that Rayleigh's analysis can be translated to apply to our diblock copolymer system.[19] In this section we focus our attention on the behavior at the very late stages of annealing. On a homogeneous substrate the main process observed is island coalescence, with bigger islands growing at the cost of smaller islands. The driving force for coalescence is the decrease of the total edge length of the islands. In our case the islands that were initially formed on the HO−SAM can be absorbed by the film forming above the H_3C−SAM, thus leaving the film surface above the HO−SAM in its lowest free energy state, namely island-free. In Figure

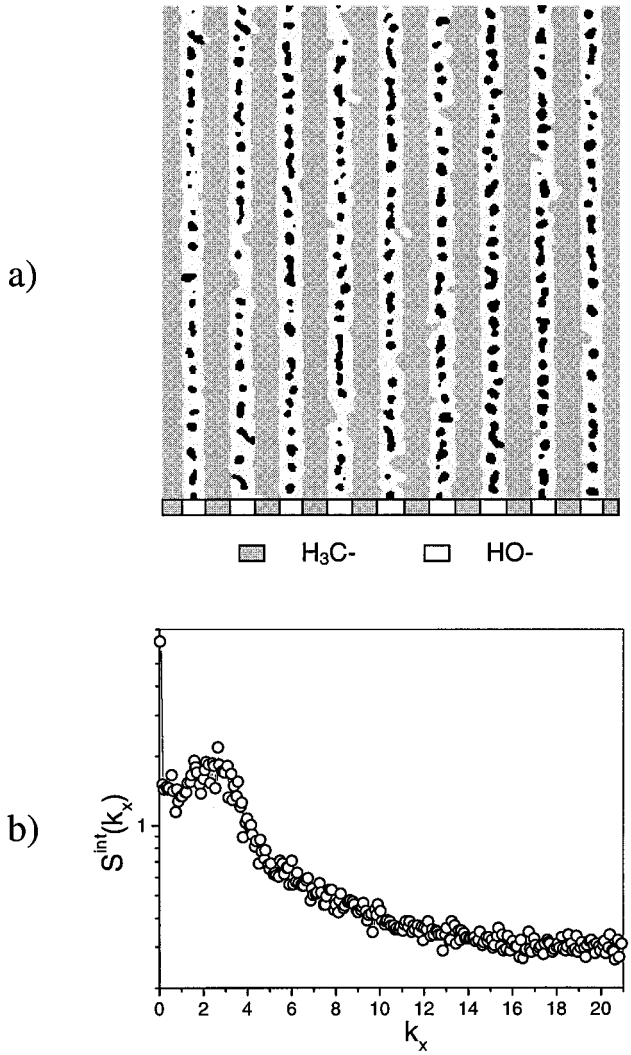

Figure 3. (a) SFM images of the time development of islands decaying on the HO−SAM stripes 3 μm in width. For clarity, we threshold the image in the following way: the absorbing film above the H_3C−SAM is gray, the $1.5L_0$ thick base layer on top of the HO−SAM is white, and islands on top of the HO−SAM are marked in black. (b) The one-dimensional Fourier transform of the image shown in (a) along the HO−SAM stripes. A peak at $k_x = 2.8\ \mu m^{-1}$ indicates a periodicity of the islands along the grating with a wavelength of $\lambda = 2.24\ \mu$m.

4 we show the late stages in the pattern evolution of the HO-terminated stripes for a grating of 8 μm periodicity (HO−SAM stripe width 4 μm). On a stripe of this width the size of the islands decreases with annealing time, and most islands disappear eventually. A plot of island radius versus annealing time as shown in Figure 5 shows a large scatter in the data. In Figure 6 we plot the total number of islands divided by initial number of islands as a function of annealing time for different HO−SAM stripe widths. For the 3, 4, and 5 μm wide HO−SAM stripes, the number of islands decreases exponentially to less than half of the initial number of islands after 30 h. No major decrease in the number of islands is observed for a HO−SAM stripe width of 6 μm (or bigger). In these cases we observe neither absorption of islands by the film above the H_3C−SAM nor "classical" island coalescence. Any explanation of the shrinkage of islands on the narrower HO−SAM stripes must also explain why islands do not shrink or coalesce on wider ones.

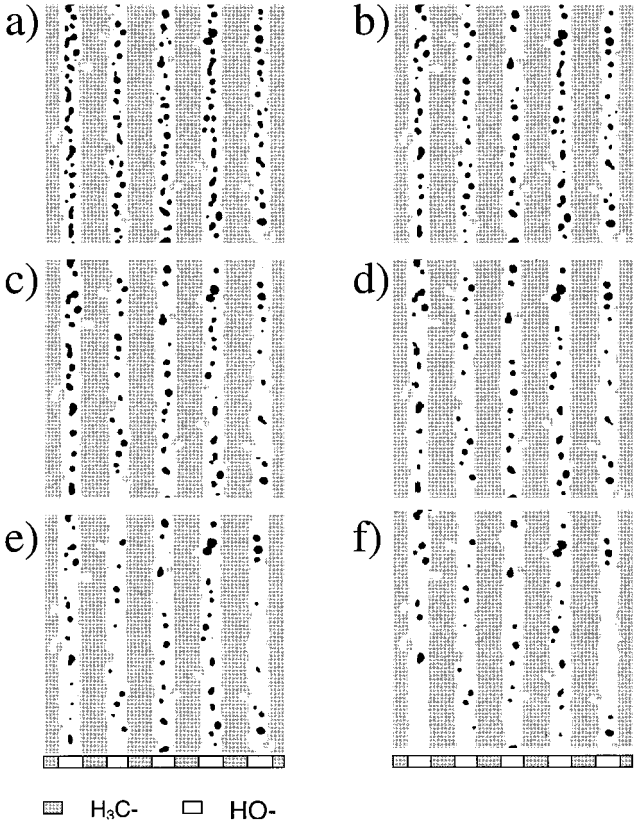

Figure 4. SFM images of the time development of islands decaying on the HO−SAM stripes with a width of 4 μm. For clarity, we threshold the image in the following way: the absorbing film above the H_3C−SAM is gray, the $1.5L_0$ thick base layer on top of the HO−SAM is white, and islands on top of the HO−SAM are marked in black. Annealing times are (a) 8, (b) 11, (c) 13.5, (d) 18.3, (e) 25.3, and (f) 47.8 h.

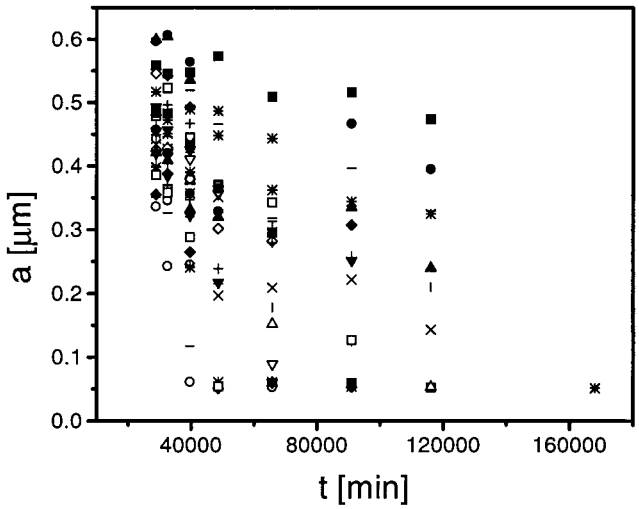

Figure 5. Time dependence of the shrinkage of islands for 30 selected islands from Figure 4. We plot the radius of the islands as measured by SFM versus the annealing time.

Usually islands are modeled as disks $1.0L_0$ in height, and with an edge line tension that provides a driving force for island shrinkage. Height profiles through the center of individual islands of different sizes are shown in Figure 7. The profiles show that the island edges are not steep as assumed in previous models[4,6] but are rather smeared out. Within these edges the film does not possess a quantized thickness of either $1.5L_0$ or $2.5L_0$. Lamellae must be either distorted from their

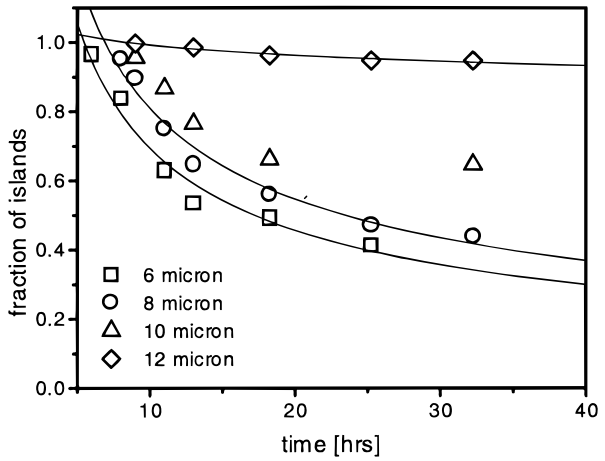

Figure 6. Number of islands divided by initial number of islands versus time for grating periodicities of 6, 8, 10, and 12 μm (HO−SAM stripe widths of 3, 4, 5, and 6 μm). The lines show an exponential decrease in island fraction.

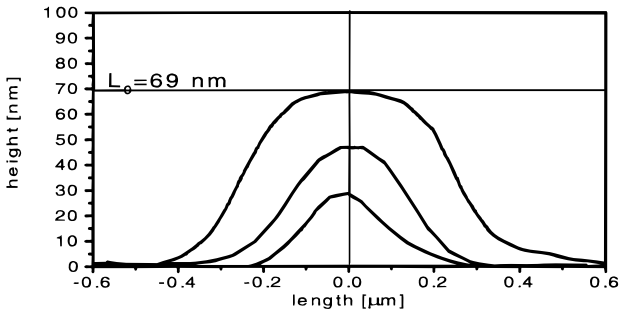

Figure 7. Height profiles of single line SFM scans through the center of islands of different radii.

equilibrium thickness or oriented perpendicular to the substrate.[9] Islands smaller than 0.5 μm in diameter cannot maintain their height of $1.0L_0$. Connected with this island shrinkage we expect a major change in morphology. In Figure 8 we show plan-view TEM images of islands of different sizes. The island edge (the region where lamellae are oriented perpendicular to the substrate) extends over a relatively large distance. Some islands of smaller size show an even more interesting morphology. In Figure 8c we show the plan-view TEM image of an island in which all of the lamellae are flipped into a perpendicular orientation.

Model

The striped geometry allows us to quantify the processes by which the islands lose single block copolymer molecules to the absorbing layer on the H_3C−SAM. We consider an isolated island next to an absorbing linear boundary and assume no influence of other islands whatsoever. The fastest transport process determines the shrinkage law. We assume that the absorption rate at the HO/H_3C−SAM boundary is not the rate-limiting process. We have to consider how single copolymer molecules leave the island and how single copolymer molecules move from the island to the absorbing boundary.

In the following we consider shrinkage of islands driven by the two-dimensional pressure in the continuous layers below the island layer as described by Nyrkova and Semenov.[8] Here we will apply the dynamic equations to the situation of a disk shaped island in the vicinity of an infinitely large island or wall. The islands at this stage always conserve their circular shape (e.g., Figure 4). This observation indicates the island edges

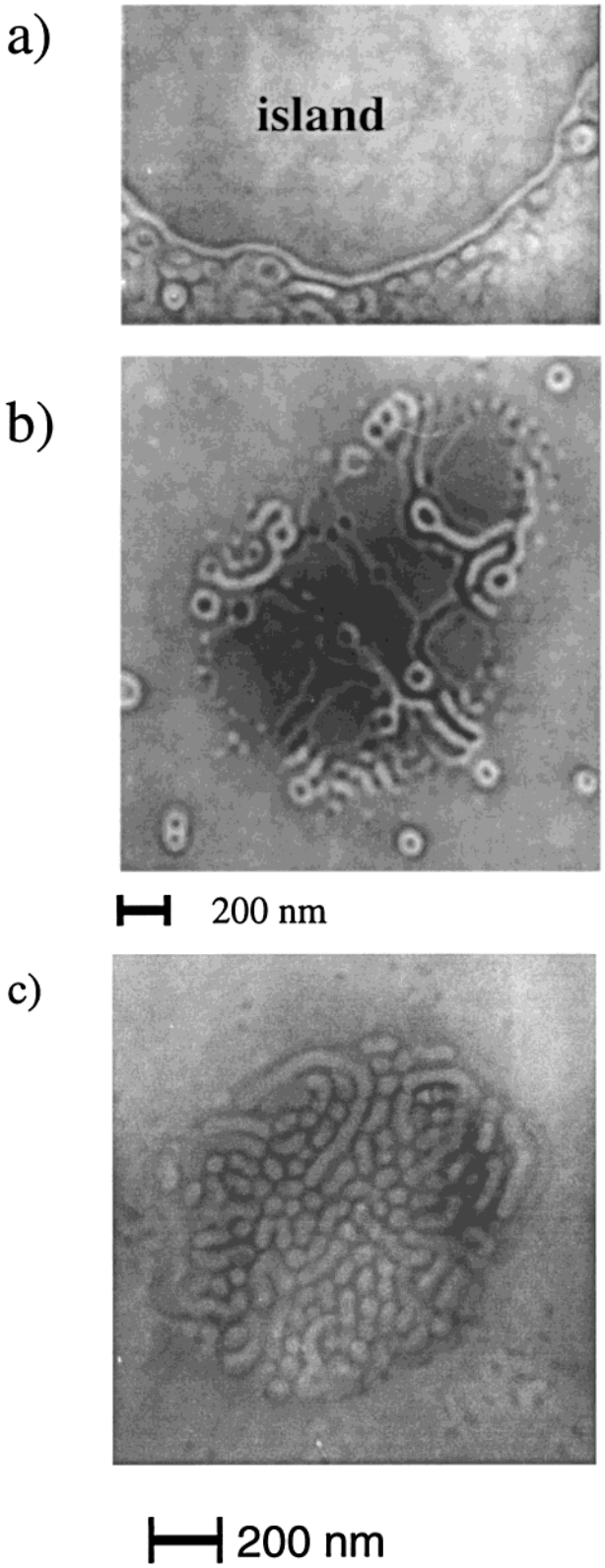

Figure 8. Plan-view TEM of islands with different radii. Islands of diameters larger than 1 μm usually only show features at the edge of the island (a). For smaller islands lamellae with perpendicular orientation extend into the island (b). In an island with a radius smaller than 1 μm, all lamellae are flipped into an orientation perpendicular to the substrate (c). The darker lamellar regions correspond to PVP as it has more contrast in the TEM through iodine staining.

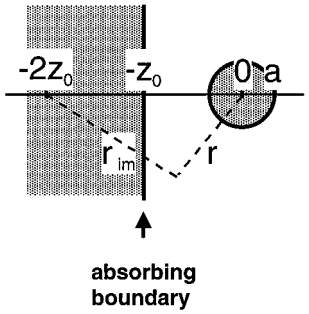

Figure 9. Variables used in the model describing a single island next to an absorbing boundary.

have a line tension τ. The three-dimensional pressure on the copolymer in an island can be written as

$$P = \frac{\tau}{a(D + L_0)} \tag{1a}$$

where a is the island radius. Usually the two-dimensional pressure is used. The three-dimensional pressure P used here contains a conversion factor of $1/(D + L_0)$, where D is the thickness of the layer through which the polymer actually flows (which is not the same as the film thickness). L_0 is the height of the island. We interpret the absorbing boundary as an infinitely large island and accordingly assume a pressure of

$$P = 0 \tag{1b}$$

acting at that boundary. The pressure difference between the vicinity of an island and the absorbing boundary will lead to a viscous flow in the underlying film. The geometry and the variables controlling the flow are illustrated in Figure 9. Using the lubrication approximation,[20,21] we get

$$\vec{j} = -\frac{1}{3\eta} D^3 \nabla P \tag{2}$$

for the total two-dimensional flux $\vec{j}$, where D is the thickness through which flow occurs as in eq 1a and η is the layer sliding viscosity.[22] Imposing mass conservation in the region exterior to islands,

$$\vec{\nabla}, \vec{j} = 0 \tag{3}$$

we get the two-dimensional Laplace equation for the pressure distribution:

$$\nabla^2 P = 0 \tag{4}$$

The solution of (4) with the boundary conditions (1) leads to the following solution for the pressure P:

$$P = \frac{\tau}{(D + L_0)a} \frac{\ln(r/r_{\text{im}})}{\ln(a/2z_0)} \tag{5}$$

where r is the distance from the center of an island located z_0 from the absorbing boundary and r_{im} is the distance to the center of an image island over the H_3C-SAM as shown in Figure 9. The pressure gradient causes a radial material flux at the boundary of an island L_0 high:

$$j_r = -L_0 \frac{\mathrm{d}a}{\mathrm{d}t} \tag{6}$$

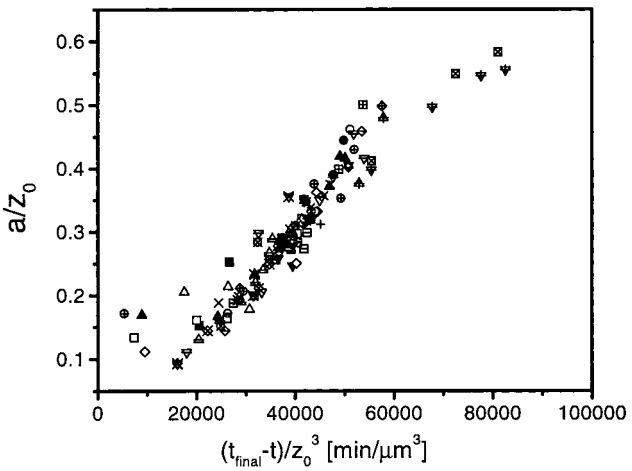

Figure 10. Plot of the shrinkage of islands on a grating with a 4 μm HO−SAM stripe width. The islands are the same as the islands plotted already in Figure 5. Here we plot the dimensionless variable a/z_0 versus the scaled time $(t_{\text{final}} - t)/z_0^3$, where a is the island radius, z_0 the distance from its center from the boundary, and t_{final} the annealing time where the island disappears. As seen, they all fall onto a single master curve.

Assuming that all material being absorbed by the film above the H_3C-SAM originates from an isolated island, the knowledge of the flux at the outer boundary allows us to determine the total flux of copolymer leaving the island. Thus, we can determine the time evolution of its radius a until the time t_{final} when the island completely disappears. We find a differential equation (8) in the scaled variables u and T:

$$u \equiv a/z_0 \tag{7a}$$

$$T \equiv \frac{\tau}{3\eta} \frac{D^3}{L_0 (L_0 + D)} \frac{t_{\text{final}} - t}{{z_0}^3} \tag{7b}$$

$$\frac{\mathrm{d}u}{\mathrm{d}T} = -\frac{1}{u^2 \ln(u/2)} \tag{8}$$

The scaled radius u of an island is simply its radius divided by the distance of its center from the absorbing boundary. Note that eq 8 is independent of the distance to the absorbing boundary.

In Figure 10 we replot the highly scattered raw data shown in Figure 5 using the variables u (eq 7a) versus time scaled by the distance to the wall cubed (the same scaling as T, see eq 7b). The data collapse considerably to approach a single curve on this plot. The major reason for the scatter in Figure 5 is thus the strong dependence of the island shrinkage rate on its position z_0 with respect to the absorbing boundary. Plotting the rescaled data corrects for this dependence.

In the discussion we will argue that a plausible choice for D is $0.5L_0$. Note that with this assumption it is possible to extract the ratio of line tension to sliding viscosity from the data in Figure 10. It could be interesting to discuss this in combination with a model for the line tension,[19] but for now it is too much of a digression. The data show that the simplification to ignore the other islands and the second boundary works very well; i.e., there is little scatter in the data. In this simplification we ignore at least two length scales, i.e., the separation between the two absorbing boundaries and the distance between the islands. Then we are left

with the distance to the boundary as the only scale, which leads to the scaling in eq 8. To examine the effect of the other boundary and other islands, we need to consider the solution to eq 4 in this geometry. This solution consists of multiple images with alternating sign. A preliminary analysis indicates that the second boundary generates a sequence of positive and negative images (sources and sinks) which largely cancel; thus, we find relatively small corrections to the one-island/one-wall solution.

Even though we find a remarkable data collapse, the smaller islands do not quantitatively follow the predictions of eq 8. A constant edge tension τ as the driving force for island shrinkage should lead to an accelerated shrinkage rate as the islands become smaller. In contrast, we observe that the shrinkage rate slows down as the islands become smaller.

The assumption that the edge tension τ is a constant, independent of island radius a, is not likely to be correct. Figure 8a shows a plan-view TEM image of the edge of a rather large island. We observe a transition edge zone from the film thickness of $1.5L_0$ to the island film thickness $2.5L_0$. The transition zone carries excess free energy, giving rise to the line tension.

There are two roughly equal contributions to the line tension. The first is the internal free energy of the island edge where the island thickness is less than L_0. As a result, copolymer chains in parallel lamellae are compressed or lamellae are flipped to become perpendicular to the substrate, both producing excess free energy. The second contribution is from the excess free energy due to excess surface associated with the edge height profile. The shape of the edge, and thus the line tension, is a compromise that roughly equalizes these two contributions.

We expect that as the island shrinks, and its height decreases below L_0, that both these contributions decrease, leading to a decreasing τ with decreasing island radius a. Indeed it is clear from the height profiles in Figure 7 that the excess surface associated with the island edge decreases as it shrinks. Furthermore, the changes in edge and internal island lamellar morphology as the island shrinks that are seen in Figure 8 will decrease the excess internal free energy of the island.

Finally, at an island radius where all the lamellae have flipped perpendicular to the substrate (Figure 8c), there is no longer much distinction to be made between edge and bulk island internal structure. The driving force now for shrinkage is primarily the surface tension. Thus, as the island shrinks, its line tension should decrease. A more detailed and quantitative theoretical analysis bears out this expectation.[19]

Discussion

We have presented results on the formation and dissolution of islands on chemically patterned surfaces. The simplified geometry reveals features that are not easily observed in an ensemble of islands on a homogeneous substrate.

From the rate of island dissolution from single chains being incorporated by an absorbing wall, we isolate the mechanism responsible for the polymer chain motion. In a model that assumes two-dimensional pressure relaxation as the main (or rate limiting) mechanism of transport, the measured island radii should collapse onto one master curve when plotted on scaled axes. We indeed find these data collapse experimentally. We exclude diffusion of domains as a whole as a possible mechanism. The center of an individual island always remains at its initial position. If desorption of single copolymer chains into the underlying polymer layer or the absorption into the film above the H_3C-SAM were the rate-limiting steps, we would not expect data collapse when these data are scaled to produce the variables u and T. In such circumstances the rate of island shrinkage would not depend on the island coordinates with respect to the H_3C-SAM boundary, whereas the opposite is true. Also, an estimate of the tunneling rate of individual PS−PVP chains through a lamellar PS−PVP layer reveals that this process is very unlikely as the tunneling rate is proportional to $\exp(-0.5\chi N)$,[23] where N is the total degree of polymerization of the copolymer. Since $\chi \approx 0.1$ and $N = 2000$, the tunneling rate would be scaled roughly by a factor of $\exp(-100)$ for the block copolymer used in this experiment.

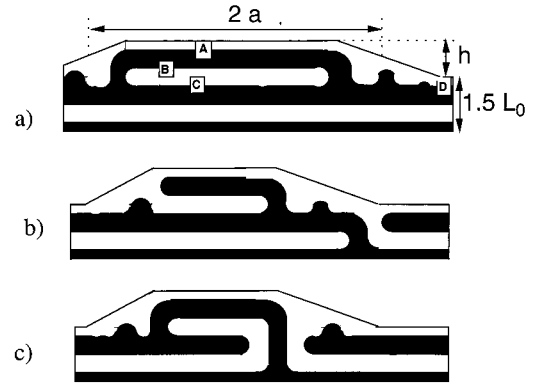

Figure 11. Proposed possible domain-edge structures. In (a) we show a conformation in which single copolymer chains in layer B are trapped within the island. The defect structures depicted in (b) and (c) allow for flow of polymer out of the island. The dark regions correspond to PVP, and the white regions correspond to PS.

Thus, the question remains to be answered how single copolymer chains travel into the underlying lamellar film. The TEM image in Figure 8a suggests an island morphology depicted schematically in Figure 11a. Even though copolymers from layer A can flow easily into layer D, copolymer from layer B can only flow into layer C. Indeed, the island shown is only typical of rather large islands. Islands of this size develop only on the HO−SAM stripes with a width larger than 3 μm, and they do not shrink as readily as smaller islands (compare Figure 6).

In contrast, smaller islands (Figure 8b) possess considerably more defects. From the different contrasts of single defects in the TEM image we conclude that some defects are only located within the island, while others extend far into the $1.5L_0$ thick base film. We support this idea with another plan-view TEM image shown in Figure 12. Here we depict a film section above an HO−SAM stripe next to an absorbing wall that has been annealed for 72 h. In an earlier stage, this film section contained islands, but the material in these islands has now been absorbed. Nevertheless, we observe defects consisting of perpendicular lamellae within the $1.5L_0$ thick film. A more realistic model of the island morphology for smaller islands is shown in Figure 11b,c. Convectional flow of copolymer chains can occur through these defect structures. As long as they have such a morphology, these islands can shrink by a pressure

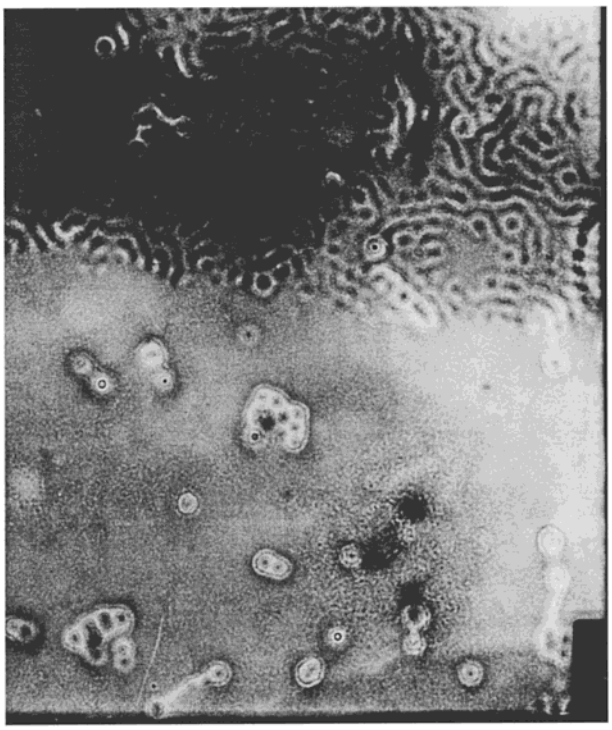

Figure 12. Plan-view TEM of a $1.5L_0$ thick PS−PVP film above the HO−SAM stripe. On the top third of the image we see a somewhat higher film above a H_3C−SAM stripe. The film above the HO−SAM does not show any surface features. All the defects lie within the film.

driven flow. The fact that some islands, particularly those with larger initial radii, do not shrink appreciably simply reflects the fact that they have a domain morphology that does not permit shrinkage by copolymer flow. Conversely, we expect that the smallest islands which have highly defective internal microstructures typified by Figure 8c will always shrink and ultimately disappear since their defect structure readily permits convective flow of block copolymer chains into the underlayer and hence to the H_3C−SAM. The experiments also show that this hypothesis is correct. From the fact that the islands are stable if large enough, it seems plausible that the flow of polymer outside the islands (in the case of the smaller ones) only takes place in one half layer. Penetration to deeper layers will probably be even harder compared to block copolymer penetration from a large island to the layer right below it.

As the islands become smaller, the free energy per unit volume becomes very large due to the line tension. As a consequence, the island height can decrease below $1.0L_0$ in order to decrease the free energy. This causes the lamellae within the center of the island to flip into a perpendicular orientation (see Figure 8c). As a final observation, we note that a large part of the data presented in Figure 10 corresponds to islands with a significantly decreased height. The island shape can be far from disklike (see Figure 7), so we expect the model of a disk shaped island to break down for the small sizes. Nevertheless, the scaling derived from the assumption of disk-shaped islands works well even for smaller islands (see Figure 10). Apparently, the same scaling applies to the limit of small islands as well.

In summary, we have been able to infer the transport mechanisms that operate to allow island shrinkage and the morphological changes necessary as islands shrink in height. We identify 2-dimensional pressure relaxation in the underlying coherent layer as the rate-determining step. All data collapse onto a master curve by plotting the island radius a divided by its distance from the wall z_0 versus $(t_{final} - t)/z_0^3$, where t_{final} is the time after which the island has disappeared. For this transport to occur, defects within the lamellar structure need to be present, so copolymer chains can flow into the underlying polymer film. These defects are present at the edges of an island, where the film thickness differs significantly from one lamellar period L_0.

Acknowledgment. We gratefully acknowledge primary funding for this work from the NSF-DMR Polymers Program (Grant DMR-9803738) and by the NSF-DMR Theory Program (Grant DMR-9870785). This work also made use of the MRL Central Facilities at UCSB that are funded by the NSF under Award DMR96032716. Part of this work was performed at the Cornell Nanofabrication Facility (a member of the National Nanofabrication Users Network) which is supported by the NSF under Grant ECS-9319009. J.G. thanks Netherlands Organization for Scientific Research (NWO) for financial support.

References and Notes

(1) Bates, F. S.; Fredrickson, G. H. *Annu. Rev. Phys. Chem.* **1990**, *41*, 525.
(2) Coulon, G.; Russell, T. P.; Deline, V. R.; Green, P. F. *Macromolecules* **1989**, *22*, 2581.
(3) Coulon, G.; Ausserre, D.; Russell, T. P. *J. Phys. (Paris)* **1990**, *51*, 777.
(4) Coulon, G.; Collin, B.; Ausserre, D.; Chatenay, D.; Russell, T. P. *J. Phys. (Paris)* **1990**, *51*, 2801.
(5) Maaloum, M.; Ausserre, D.; Chatenay, D.; Coulon, G.; Gallot, Y. *Phys. Rev. Lett.* **1992**, *68*, 1575.
(6) Coulon, G.; Collin, B.; Chatenay, D.; Gallot, Y. *J. Phys. II* **1993**, *3*, 697.
(7) Lifshitz, I. M.; Slyozov, V. V. *J. Phys. Chem. Solids* **1961**, *19*, 35.
(8) Nyrkova, I. A.; Semenov, A. N. *Polym. Prepr. (Am. Chem. Soc., Div. Polym. Chem.)* **1994**, *35*, 564.
(9) Carvalho, B. L.; Thomas, E. L. *Phys. Rev. Lett.* **1994**, *73*, 3321.
(10) Grim, P. C. M.; Nyrkova, I. A.; Semenov, A. N.; ten Brinke, G.; Hadziioannou, G. *Macromolecules* **1995**, *28*, 7501.
(11) Heier, J.; Kramer, E. J.; Walheim, S.; Krausch, G. *Macromolecules* **1997**, *30*, 6610.
(12) Rockford, L.; Liu, Y.; Mansky, P.; Russell, T. P.; Yoon, M.; Mochrie, S. *Phys. Rev. Lett.* **1999**, *82*, 2602.
(13) Böltau, M.; Walheim, S.; Mlynek, J.; Krausch, G.; Steiner, U. *Nature* **1998**, *391*, 877.
(14) Karim, A.; Douglas, J. F.; Lee, B. P.; Glotzer, S. C.; Rogers, J. A.; Jackman, R. J.; Amis, E. J.; Whitesides, G. M. *Phys. Rev. E* **1998**, *57*, R6273. Ermi, B. D.; Nisato, G.; Douglas, J. F.; Rogers, J. A.; Karim, A. *Phys. Rev. Lett.* **1998**, *81*, 3900.
(15) Matsushita, Y.; Shimizu, K.; Nakao, Y.; Choshi, H.; Noda, I.; Nagasawa, M. *Polym. J.* **1986**, *18*, 361.
(16) Kumar, A.; Whitesides, G. M. *Langmuir* **1991**, *7*, 1013.
(17) Heier, J.; Kramer, E. J.; Bates, F. S.; Krausch, G. *J. Chem. Phys.* **1999**, *111*, 11101.
(18) Lord Rayleigh, *Proc. London Math. Soc. (London)* **1863**, *275*, 47.
(19) Groenewold, J. Unpublished work.
(20) Faber, T. E. *Fluid Dynamics for Physicists*; Cambridge University Press: New York, 1995; p 214.
(21) Koneripalli, N.; Bates, F. S.; Fredrickson, G. H. *Phys. Rev. Lett.* **1998**, *81*, 1861.
(22) deGennes, P.-G.; Prost, J. *The Physics of Liquid Crystals*; Oxford University Press: New York, 1993.
(23) Yokoyama, H.; Kramer, E. J.; Rafailovich, M. H.; Sokolov, J.; Schwarz, S. A. *Macromolecules* **1998**, *31*, 8826.

MA991649V